PCCP

RSC Publishing

PAPER

View Article Online
View Journal | View Issue

Cite this: *Phys. Chem. Chem. Phys.*, 2013, **15**, 12220

Three-dimensional B,N-doped graphene foam as a metal-free catalyst for oxygen reduction reaction†

Yuhua Xue,‡[ab] Dingshan Yu,‡[b] Liming Dai,*[ab] Ruigang Wang,[c] Dingqiang Li,[c] Ajit Roy,[d] Fan Lu,[a] Hao Chen,[a] Yong Liu*[a] and Jia Qu*[a]

Received 8th May 2013,
Accepted 9th May 2013

DOI: 10.1039/c3cp51942b

www.rsc.org/pccp

Using a modified chemical vapor deposition (CVD) method, we have prepared a class of new graphene foams (GFs) doped with nitrogen, boron or both. Nitrogen-doped graphene foams (N-GFs) with a nitrogen doping level of 3.1 atom% were prepared by CVD of CH_4 in the presence of NH_3 while boron-doped graphene foams (B-GFs) with a boron doping level of 2.1 atom% were produced by using toluene and triethyl borate as a carbon and a boron source. On the other hand, graphene foams co-doped with nitrogen (4.5 atom%) and boron (3 atom%) (BN-GFs) were prepared by CVD using melamine diborate as the precursor. In all cases, scanning electron microscope (SEM) images revealed well-defined foam-like microstructures, while electrochemical measurements showed much higher electrocatalytic activities toward oxygen reduction reaction for the doped graphene foams than their undoped counterparts.

1. Introduction

Graphene, two-dimensional (2D) single-atomic layer graphite, has been demonstrated to show superior thermal, electrical, and mechanical properties,[1–5] along with a high surface area.[6] Due to the presence of strong covalent bonding in the carbon plane and the much weaker van der Waals interaction in the transverse direction between the layers, graphene-based materials exhibit strong direction-dependent thermal and electrical transport properties with extremely low out-of-plane conductivities. In order to extend the unique properties of graphene into the third dimension, we have recently prepared 3D pillared carbon nanotube (CNT)–graphene networks comprising alternating layers of graphene sheets and vertically-aligned carbon nanotubes (VA-CNTs) to facilitate thermal/electrical transport along both in-plane as well as out-of-plane directions with respect to the graphene sheets.[7] These inherently nanoporous 3D pillared VA-CNT-graphene architectures with large surface areas have been demonstrated to be useful electrode materials for advanced supercapacitors.[7]

Recently, Chen and co-workers[8] have reported on the development of graphene foams (GFs), a new class of 3D graphene-based materials. Similar to the 3D pillared VA-CNT-graphene architectures, the unique 3D network structure, high specific surface area and excellent electrical and mechanical properties of GFs should also enable a wide variety of exciting applications, including new materials for energy conversion and storage, thermal management, potential high-performance nano/microscale integrated devices, multifunctional materials for aerospace systems, security sensors, to name a few. To our best knowledge, however, the possibility for preparing graphene foams doped with hetero-atoms (*e.g.*, N-doping, B-doping, or N and B co-doping; designated as: N-GF, B-GF or BN-GF) by the CVD method has not been exploited. The doping of GFs with heteroatoms, if realized, should further extend their potential applications, as demonstrated by recent work on carbon nanotubes and graphene doped with hetero-atoms, including N and B, for oxygen reduction with high electrocatalytic activity, long-term operation stability, and tolerance to methanol crossover/CO-poisoning effects.[9–11] By modifying the CVD method reported by Chen and co-workers,[8] we successfully prepared the N-GF, B-GF, and BN-GF materials. Herein, we report the synthetic procedures, along with the structural and property characterization of the resultant 3D B,N-doped graphene foams

[a] *Institute of Advanced Materials for Nano-Bio Applications, School of Ophthalmology & Optometry, Wenzhou Medical College, 270 Xueyuan Xi Road, Wenzhou, Zhejiang 325027, China. E-mail: yongliu1980@hotmail.com, jia.qu@163.com*

[b] *Center of Advanced Science and Engineering for Carbon (Case4Carbon), Department of Macromolecular Science and Engineering, Case Western Reserve University, Cleveland, Ohio 44106, USA. E-mail: liming.dai@case.edu*

[c] *Department of Chemistry, Youngstown State University, One University Plaza, Youngstown, Ohio 44555, USA*

[d] *Thermal Science and Materials Branch, Materials & Manufacturing Directorate, Air Force Research Laboratory, Dayton, OH 45433, USA*

† Electronic supplementary information (ESI) available: Raman, and CV curves for glass carbon, GF, B-GF, N-GF and BN-GF in Fig. S1 and S2. See DOI: 10.1039/c3cp51942b

‡ These authors contributed equally to this work.

as well as the detailed demonstration of their use as metal-free oxygen reduction reaction (ORR) electrocatalysts.

2. Experimental

Preparation of graphene foams (GFs) and N-doped graphene foams (N-GFs) by CVD

The heteroatom-free pure carbon graphene foams (GFs) were produced according to the reported method.[8] Detailed procedures for preparing the N-GFs are as follows: to start with, a nickel foam (INCO, Advanced Technology Materials (Dalian) Co., Ltd. Pore size: 590 μm) was heated up to 1000 °C in a horizontal quartz tube under Ar (500 standard cubic centimeters per minute (SCCM)) and H_2 (200 SCCM) and kept *in situ* for 5 min to clean up its surface and remove a thin surface oxide layer, if any. CH_4 (10 SCCM) and NH_3 (10 SCCM) were then introduced into the tube and kept flowing for 5 min. The graphene coated nickel foam was then rapidly moved away from the furnace center (1000 °C) under Ar protection. Upon cooling down to room temperature (20 °C), the Ni foam covered with N-doped graphene was taken out of the furnace tube and drop-coated with a poly(methyl methacrylate) (PMMA) solution (6 M in toluene), and then dried at 180 °C for 30 min, resulting in the formation of a thin PMMA film on the graphene surface (PMMA/N-GF@Ni) to prevent possible structural failure of the resultant N-GF when the nickel template was etched away. Then, nickel was removed by immersing the sample in a HCl (3 M) solution at 70 °C for 5 h to obtain PMMA/N-GF. Finally, the free-standing N-GF was obtained by dissolving the PMMA protective layer in hot acetone at 55 °C.

Preparation of B-doped graphene foams (B-GFs) by CVD

B-GFs were grown by the conventional CVD method using toluene and triethyl borate as a carbon and a boron source, respectively.[10] Typically, a nickel foam was heated up to 1000 °C in a horizontal quartz tube under Ar (500 SCCM) and H_2 (200 SCCM) and kept *in situ* for 5 min to clean up its surface. Then, a toluene solution (1 ml) containing 1 wt% triethyl was injected within 5 minutes. After the growth process was completed, the B-graphene foam was quickly removed and subjected to the same treatment as described above to remove the nickel template.

Preparation of graphene foams co-doped with N and B (BN-GFs) by CVD

Melamine diborate, synthesized by reacting melamine with boric acid,[10] was used as a precursor for synthesizing BN-GF by thermal CVD. Briefly, melamine diborate was prepared by first dissolving melamine (1 mmol) in deionized water at 80 °C, and then boric acid (2 mmol) was added slowly and the temperature was maintained at 80 °C for 30 min under stirring. Thereafter, the mixture solution was cooled down slowly to allow complete precipitation of melamine diborate, followed by filtration and overnight drying at 80 °C. The same nickel foam used for synthesizing N-GF by CVD was used as the template for the preparation of BN-GF. In a typical CVD process, the melamine diborate precursor and nickel foam were placed inside a quartz tube furnace. Then, the temperature of the furnace was ramped to 1000 °C under an Ar/H_2 flow (100 : 100 SCCM). Thereafter, the nickel foam substrate was quickly moved into the 1000 °C region for 5 minutes for surface cleaning. Then, nitrogen gas was introduced into the quartz tube and melamine diborate was moved into the relatively low temperature region (about 500 °C) and kept for 3 minutes to grow the BN-GF. Upon completion of the growth process, the resultant BN-GF supported by the nickel substrate was removed quickly from the reaction zone and cooled down to room temperature under Ar flow. The resultant BN-GF covered onto the Ni foam substrate was subjected to the same PMMA and HCl treatments to remove the nickel template, as is the case for N-GF (*super infra*).

Characterization

Transmission electron microscopy (TEM) was carried out using a JEOL2100 high resolution transmission electron microscope operating at an acceleration voltage of 200 kV. Scanning electron microscope (SEM) imaging was performed using a JEOL JSM-6510LV scanning electron microscope. SEM energy-dispersive X-ray (EDX) mapping was performed on a Focused Ion Beam Scanning Electron Microscope (JIB 4500 MultiBeam). X-ray photoelectron spectroscopic (XPS) measurements were performed on a VG Microtech ESCA 2000 using a monochromic Al X-ray source (97.9 W, 93.9 eV). X-ray diffraction (XRD) was performed on a Miniflex Desktop X-ray Diffractometer. Fourier transform infrared spectra (FITR) were recorded on a PerkinElmer spectrum GX FTIR system. The thermogravimetric analysis (TGA) was carried out on a TA instrument with a heating rate of 10 °C in nitrogen. The Raman spectra were collected by the Raman spectroscopy (Renishaw), using 514 nm laser.

Electrochemical measurements

Electrochemical measurements were conducted on a computer-controlled potentiostat (CHI 760C, CH Instrument, USA) with a three-electrode electrochemical cell. A platinum wire was used as the counter electrode and a saturated calomel electrode (SCE) as the reference electrode. All the experiments were conducted at room temperature (25 ± 1 °C). Graphene foam was directly transferred onto the GC electrode, followed by casting with a Nafion solution (0.05 wt% in isopropanol) as the binder. Prior to electrochemical measurements, all the electrode materials were subjected to the electrochemical purification to completely remove the metal catalyst residues, if any, according to the published procedure.[9] The activity of the electrocatalysts was evaluated by the cyclic voltammetry and linear sweep voltammetry techniques on rotating disk electrodes (RDE). Durability testing of the BN-GF electrode and the Pt/C electrocatalyst (Pt–C, Pt: 45 wt%, Vulcan XC-72R) was conducted by the chronoamperometric technique at −0.25 V (*vs.* SCE) in an oxygen-saturated aqueous solution of 0.1 M KOH for up to 20 000 s. As the newly developed 3D metal-free ORR catalysts showed very high electrocatalytic activities, we want to use the commercial electrode with the highest Pt content (45 wt% Pt, and hence the highest catalytic

activity) as reference, rather than the commonly used Pt–C, Pt: 20 wt%, Vulcan XC-72R.

3. Results and discussion

Fig. 1 shows photodigital images of a nickel foam before (Fig. 1a) and after (Fig. 1b) the growth of GF co-doped with B and N elements. Fig. 1c is the scanning electron microscope (SEM) image of pure GF. Fig. 1d–f reproduce the SEM images of the B-doped, N-doped, and B,N co-doped GF, respectively; all show well-defined foam-like microstructures.

To investigate effects of the heteroatom-doping on graphene foams, Raman spectra of all the as-prepared graphene foams were measured (Fig. 2a and Fig. S1 in ESI†). As can be seen in Fig. 2a, a D-band at 1365 cm^{-1} was observed for all the doped graphene foams because of the disordered carbon structures caused by incorporating heteroatoms into the graphene structure. In contrast, there is no D-band for GF, indicating a well ordered graphitic structure for the pure graphene foam. An about 6 cm^{-1} shift of the G band for the pure graphene foam (1581 cm^{-1}) to the G band of BN-GF (1587 cm^{-1}) was observed due to the structural distortion of graphene associated with different bond lengths of C–C, C–N, and C–B induced by doping,[12,13] while the B–N mode in BN-GF overlapped with the D band.[14,15] The appearance of a relatively weak 2D-band at 2720 cm^{-1} suggests that the as-prepared GF contains mainly a few layered graphene sheets, though the presence of single-layer graphene sheets cannot be ruled out (*vide infra*). The appearance of a D′ band at 1620 cm^{-1} is attributable to the distortion of the graphene crystal size or lattice induced by the B and/or N doping.[16,17]

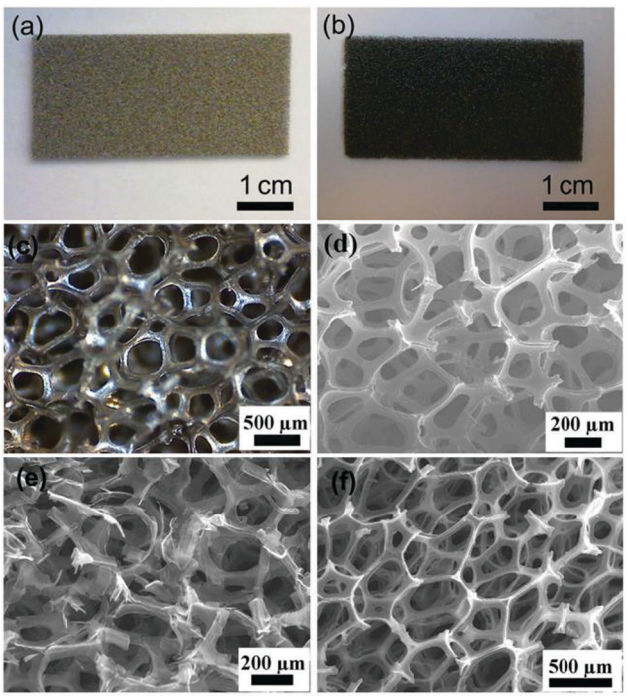

Fig. 1 Photographs of a nickel foam template (a) before and (b) after the growth of BN-GF, and (c) SEM image of a free-standing GF after removing the nickel template. SEM images of (d) B-GF, (e) N-GF, and (f) BN-GF.

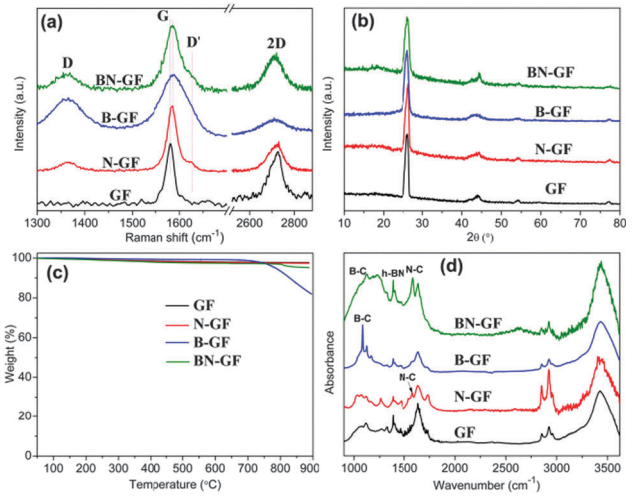

Fig. 2 (a) Raman spectra, (b) XRD profiles, (c) TGA curves, and (d) FTIR spectra of GF, N-GF, B-GF, and BN-GF.

While the X-ray diffraction (XRD) patterns given in Fig. 2b show a strong [002] graphitic peak at 26.5°,[18] indicating a high crystalline degree for all the graphene foams, both doped and undoped, the corresponding thermogravimetric analysis (TGA) curves in Fig. 2c show a very high thermal stability for all of them up to 900 °C. The weight loss at 900 °C for BN-GF is 4.8 wt%, which is slightly higher than pure GF (2.3 wt%) and N-GF (2.5 wt%), but still relatively lower than B-GF (18.1 wt%). This, in conjunction with the D-band intensities seen in the Raman spectra (Fig. 2a), indicates that defects in the graphitic structure play an important role in regulating their thermal stabilities, which are in the following order GF > N-GF > BN-GF > B-GF. The corresponding Fourier transform infrared (FTIR) spectra (Fig. 2d) show the C–N vibration band at 1580 cm^{-1} for both N-GF and BN-GF, along with the peaks at 1410 cm^{-1} and 1085 cm^{-1} associated with the hexagonal boron nitride (h-BN) and C–B bond, respectively, in BN-GF and B-GF. The h-BN peak at 1400 cm^{-1} for BN-GF may also overlap with the B–O mode for B-GF and BN-GF (Fig. 2d, *cf.* XPS data below).[19] The peak at 2800 cm^{-1} is attributable to C–H, indicating H-termination for the graphene foam as Ar/H_2 was used as the gas carrier during the CVD process. The peak at 3400 cm^{-1} can be assigned to –OH due to the physically adsorbed moisture from air and/or the use of a borate source as a boron precursor.

To monitor the doping levels, we carried out X-ray photoelectron spectroscopic (XPS) measurements. The XPS spectrum of the undoped GF given in Fig. 3a shows the C 1s peak, along with a very weak, but noticeable, O 1s peak. The presence of a trace amount of O in the GF sample is possibly due to the incorporation of physically adsorbed oxygen as the graphitic structure is known to be susceptible to oxygen absorption even at a low pressure.[20] For B-GF and BN-GF, the possibility for some of the O in the borate precursor to be incorporated into the resultant graphitic network cannot be ruled out.

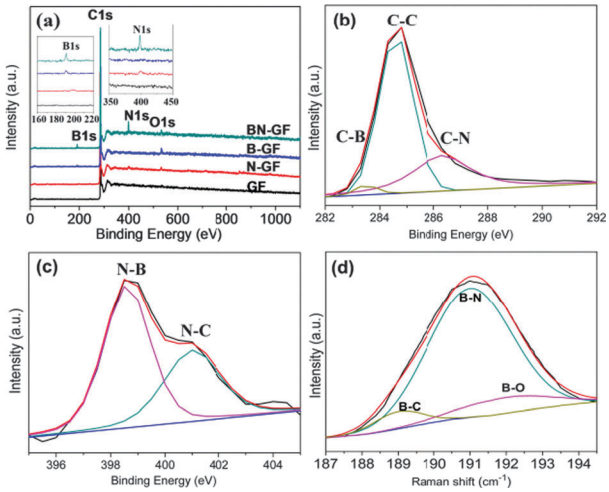

Fig. 3 (a) XPS survey spectra of GF, N-GF, B-GF, and BN-GF. Insets in (a) represent enlarged regions of the survey spectra around B 1s and N 1s peaks. High-resolution XPS spectra of (b) C 1s, (c) N 1s, and (d) B 1s for the BN-GF.

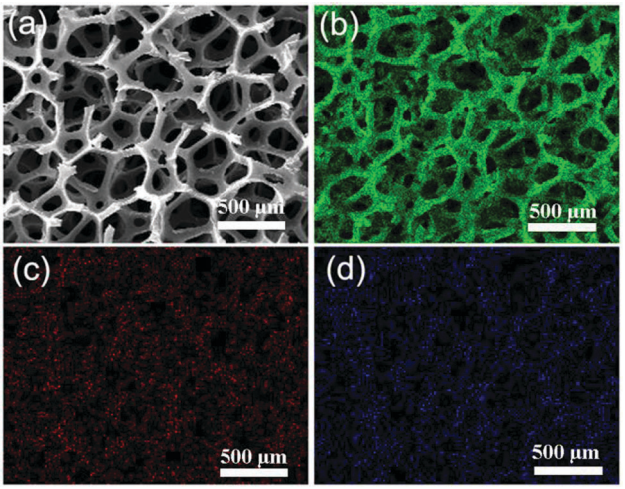

Fig. 4 (a) SEM image of BN-GF and the corresponding EDX mapping of (b) C, (c) B, and (d) N elements.

As expected, the XPS survey spectra for N-GF and B-GF show an additional N 1s and B 1s peak, respectively, while the corresponding XPS spectrum for NB-GF reveals both N 1s and B 1s peaks (Fig. 3a). From these XPS survey spectra, it was found that the N content in N-GF is 3.1 atom%, B content in B-GF is 2.1 atom%, and the N and B contents in NB-GF are 4.5 atom% and 3 atom%, respectively. The high-resolution XPS C 1s spectrum of BN-GF is given in Fig. 3b. Similar to the XPS spectra of BCN nanotubes,[10,21] the C 1s peak can be resolved into three components at 283.5 eV, 284.6 eV and 286.3 eV, attributable to the C–B, C–C and C–N bonds, respectively (no C–O in Fig. 3b for the physically adsorbed oxygen). Fig. 3c shows the high-resolution XPS N 1s peak of BN-GF, which can be fitted to two components at 398.5 eV (N–B), and 401.0 eV (N–C). The corresponding high-resolution B 1s spectrum in Fig. 3d was deconvoluted into the B–C, B–N and B–O (from the borate precursor) peaks centered at around 189, 191, and 192 eV, respectively, with the B–N being a dominant component.

Having successfully determined the chemical composition by XPS, the surface distribution of C, B, and N elements in BN-GF was investigated by energy-dispersive X-ray (EDX) mapping. As shown in Fig. 4, a uniform distribution has been achieved for all of the major constituent elements in the graphene foam.

Consistent with the Raman spectra shown in Fig. 2a, TEM images in Fig. 5 reveal that the BN-GFs are mainly composed of multilayered graphene sheets with the number of layers typically less than five (Fig. 5a and b). The selected area electron diffraction patterns (SAEDs) (inset, Fig. 5b) show sixfold symmetry peaks with the {2110} spots appearing to be more intense relative to the {1100} spots, reflecting a few layers of graphene sheets with high crystallinity.[22] Single layer graphene sheets were also observed in some cases, as indicated by the corresponding SAED pattern given in the inset of Fig. 5c, which shows typical well-defined sixfold symmetry peaks with the {1100} spots being more intense relative to the {2110} spots.[22] Fig. 5e shows typical Raman spectra for multi- and single-layered graphene sheets in the BN-GFs. Based on the above

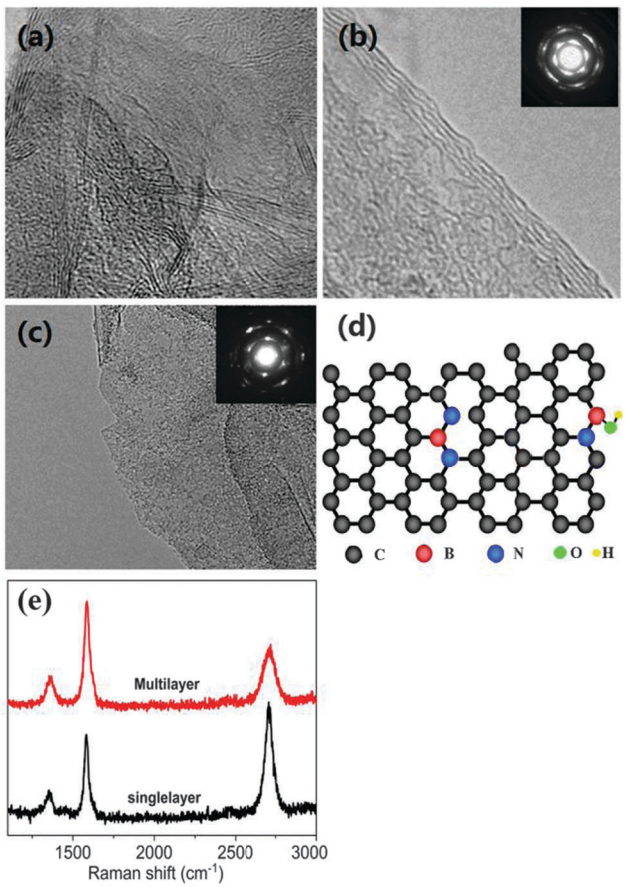

Fig. 5 TEM images of (a and b) multilayer BN-doped graphene, (c) single layer BN-doped graphene from the BN-GF. The insets in (b) and (c) are the corresponding SAED patterns in different locations. (d) The model schematic structure for BN-doped graphene with the black, blue, green and red balls representing carbon, nitrogen, oxygen and boron atoms, respectively. (e) Raman spectra of multilayer and single layer BN-doped graphene from the BN-GF.

microscopic and spectroscopic analyses, a schematic molecular structure was drawn in Fig. 5d for the BN-GF as a working model.

In view of our previous work on the use of B and N co-doped vertically-aligned carbon nanotubes (VA-BCNs) as the electrocatalysts for oxygen reduction,[10] we carried out the following electrochemical study. In particular, we compared the electrocatalytic activity toward ORR for the BN-GF with those of the undoped GF, B-GF, N-GF, and a commercial platinum–carbon catalyst (Pt–C, Pt: 45 wt%, Vulcan XC-72R) by cyclic voltammetry in an aqueous solution of N_2-saturated or O_2-saturated 0.1 M KOH solution at a scanning rate of 100 mV s^{-1} (Fig. 6). As can be seen in Fig. 6, all of the four electrodes based on graphene foam materials showed substantial reduction current in the presence of oxygen, whereas no noticeable response was observed under nitrogen. Comparison between the undoped GF and B-GF or N-GF electrodes shows that N-doping significantly improves the electrocatalytic activity towards ORR in terms of both the onset/peak potentials and the peak current. As is the case for VA-BCN,[10] the synergetic effect associated with the B- and N-co-doping made the 3D BN-GF electrode to be most active among all of the electrodes used in this study, and even slightly better than the Pt–C/GC electrode in terms of the reduction in peak current. This is because not only both the isolated N and B atoms can act as active sites for ORR through charge transfer with neighbouring C atoms,[9,11,23–25] but also interaction between adjacent N and B atoms could reduce the bandgap energy to further facilitate the ORR performance of the BN-GF electrode.[10] Besides, B- and N-co-doping could also enhance the electroactive surface area significantly (Fig. S2 and the associated discussion in ESI†). A possible influence of the oxygen incorporation into the graphitic network from the borate precursor on the ORR performance was shown to be insignificant due, most probably, to its relatively low content (Fig. 3d).

To examine possible cross-over effects, we measured the electrocatalytic selectivity of the BN-GF and the commercial Pt–C electrodes against the electrooxidation of methanol by cyclic voltammetry in an O_2-saturated 0.1 M KOH solution with 1 M methanol.[10] As can be seen in Fig. 7a, the cathodic signals toward the ORR at about −0.12 V disappeared in the CV curves of the Pt–C/GC electrode upon addition of 1 M methanol into the O_2-saturated 0.1 M KOH solution. At the same time, the current intensity corresponding to methanol oxidation at the Pt–C/GC electrode reached 7.8 mA cm^{-2} at −0.03 V. However, no obvious change was observed for the BN-GF/GC electrode under the same conditions (Fig. 7b). These results clearly indicate that the BN-GF catalyst possesses a high catalytic activity toward the ORR and is almost free from the cross-over effect.

To gain further insights into the role of the BN-GF catalyst during the ORR process, we performed linear sweep voltammetric measurements on the GF, B-GF, N-GF, BN-GF, and

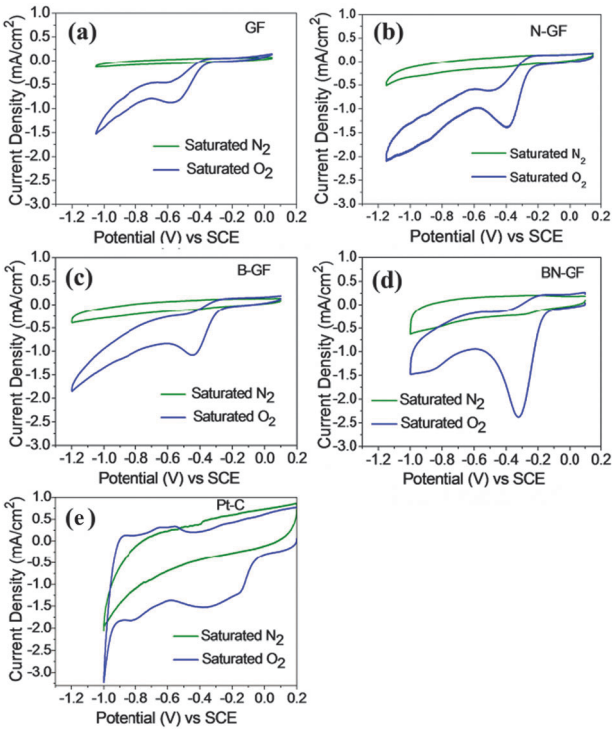

Fig. 6 Typical cyclic voltammograms for the ORR at (a) the GF/GC electrode, (b) the B-GF/GC, (c) the N-GF/GC electrode, (d) the BN-GF/GC electrode, and (e) the Pt–C/GC electrode in a N_2-saturated or O_2-saturated 0.10 M KOH solution. Scan rate: 100 mV s^{-1}.

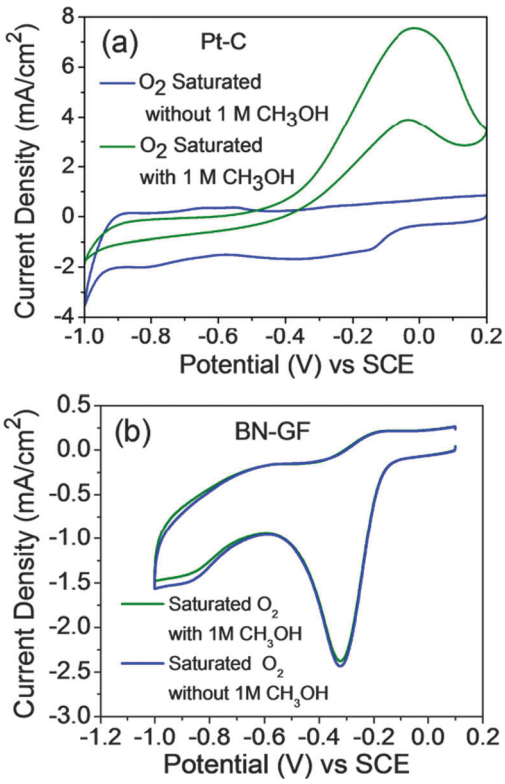

Fig. 7 Typical cyclic voltammograms for (a) the Pt–C/GC electrode and (b) the BN-GF/GC electrode in an oxygen-saturated 0.1 M KOH solution or an oxygen-saturated 0.1 M solution of KOH upon addition of CH_3OH (1 M). Scan rate: 100 mV s^{-1}.

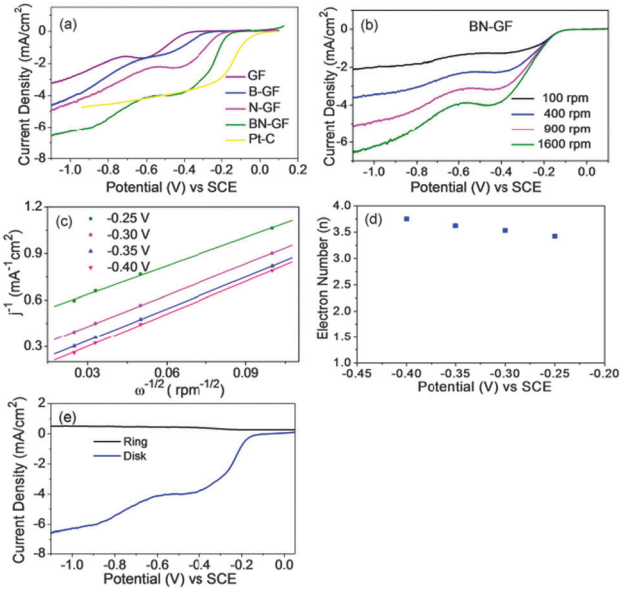

Fig. 8 (a) RDE voltammograms of the undoped GF/GC electrode, the B-GF/GC electrode, the N-GF/GC electrode, the BN-GF/GC electrode, and the Pt–C/GC electrode in an oxygen saturated 0.1 M KOH solution at a rotation rate of 1600 rpm. Scan rate: 10 mV s^{-1}. (b) RDE voltammograms of the BN-GF/GC electrode in an O_2-saturated, 0.1 M KOH solution at a scan rate of 10 mV s^{-1}, and at different rotation rates. (c) Koutecky–Levich plot of j^{-1} *versus* $\omega^{-1/2}$ at different electrode potentials of −0.25, −0.30, −0.35, and −0.40 V, (d) the dependence of transferred electron number (n) on the potential. The experimental data were obtained from (c). (e) RRDE voltammograms of the BN-GF/GC electrode in an O_2-saturated 0.1 M KOH solution at a scan rate of 10 mV s^{-1} at 1600 rpm.

the commercial Pt–C catalysts in an aqueous solution of O_2-saturated 0.1 M KOH at a rotation rate of 1600 rpm and a scan rate of 10 mV s^{-1}. As can be seen in Fig. 8a, the onset potential of the BN-GF/GC electrode for the ORR is at approximately −0.16 V, which is more positive than those of the N-GF/GC electrode (−0.19 V) and the B-GF/GC electrode (−0.28 V) as well as the undoped GF/GC electrode (−0.39 V). Besides, the diffusion current density from the BN-GF/GC electrode is also much higher than those of the N-GF/GC and GF/GC electrodes. Once again, these results indicate that the BN-GF electrocatalyst showed the highest electrocatalytic activity towards ORR among all graphene foam electrodes studied in the present work. Although the onset potential for the BN-GF/GC electrode (*ca.* −0.16 V) is still more negative than that for the Pt–C/GC electrode (*ca.* −0.01 V), the BN-GF/GC electrode exhibited a higher oxygen reduction current density with respect to the Pt–C/GC. In addition to the synergetic effect arising from the B and N co-doping, the 3D foam structure with a well-defined porosity and large surface area could have also facilitated the electrolyte/reactant diffusion to enhance the reduction current, as is the case for VA-NCNTs.[9]

We further investigated the reaction kinetics by rotating-disk voltammetry (Fig. 8b). As expected, the current density increased as the rotation rate increased (from 100 to 1600 rpm). The transferred electron number per oxygen molecule involved in the ORR process was determined by Koutecky–Levich equation, which relates the current density j to the rotation rate ω of the electrode.

$$\frac{1}{j} = \frac{1}{j_k} + \frac{1}{B\omega^{0.5}} \quad (1)$$

where j_k is the kinetic current density and B is expressed by the following expression:

$$B = 0.2nF(D_{O_2})^{2/3}\nu^{-1/6}C_{O_2} \quad (2)$$

where n represents the number of electrons transferred per oxygen molecule; F is the Faraday constant (F = 96 485 C mol^{-1}); D_{O_2} is the diffusion coefficient of O_2 in 0.1 M KOH (1.9×10^{-5} cm^2 s^{-1}); ν is the kinematic viscosity of the electrolyte solution (0.01 cm^2 s^{-1}); C_{O_2} is the concentration of dissolved O_2 (1.2×10^{-6} mol cm^{-3}). The constant 0.2 is adopted when the rotation speed is expressed in rpm.

The corresponding Koutecky–Levich plots (j^{-1} *vs.* $\omega^{-1/2}$) at various electrode potentials exhibited a good linearity (Fig. 8c), indicating a first-order reaction kinetics with respect to the concentration of dissolved O_2. The n value for the BN-GF was derived to be 3.4–3.8 at the potential ranging from −0.2 to −0.5 V (Fig. 8d), suggesting a four-electron process for ORR on the BN-GF electrode. This is further confirmed by the negligible ring current recorded at a Pt rotating ring-disk electrode[9] (RRDE, Fig. 8e).

To evaluate the stability of the BN-GF ORR catalyst with respect to the commercial Pt–C electrode, we test their stability at a constant voltage of −0.25 V for 20 000 s in a 0.1 M KOH solution saturated with O_2 at a rotation rate of 1600 rpm (Fig. 9). As can be seen, the current–time (i–t) chronoamperometric response for the BN-GF/GC electrode exhibited a very slow attenuation with a high current retention (89%) after 20 000 s. In contrast, the Pt–C/GC electrode exhibited a much faster current decrease with an approximately 40% current loss after 20 000 s. Thus, the BN-GF catalyst is more stable than the noble Pt catalyst toward ORR in alkaline medium. To examine the CO poisoning effect, a CO gas was introduced into the electrolyte. As is shown in Fig. 9b, the BN-GF/GC electrode was insensitive to CO, whereas the Pt/C electrode was rapidly poisoned under the same conditions.

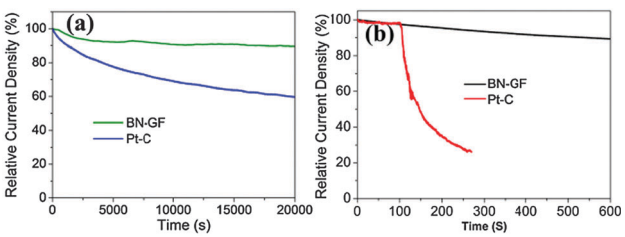

Fig. 9 (a) Current–time (i–t) chronoamperometric response of the BN-GF/GC electrode, and the Pt–C/GC electrode at −0.25 V in O_2-saturated 0.10 M KOH. (b) Current–time (i–t) chronoamperometric response of the BN-GF/GC electrode, and the Pt–C/GC electrode upon introduction of CO after about 150 s at −0.25 V.

4. Conclusions

In summary, we have demonstrated the first CVD synthesis of a new class of graphene foams (GFs) doped with nitrogen, boron or both. Various microscopic and spectroscopic investigations, including SEM, TEM, FTIR, XRD, XPS, and Raman, revealed foam-like microstructures with well-defined chemical compositions for the resultant N-GFs, B-GFs, and BN-GFs. TGA analyses indicated a good thermal stability while electrochemical measurements showed high electrocatalytic activities for oxygen reduction reaction with a higher current generation capability, better stability, and superior tolerance to the methanol crossover effect with respect to commercial platinum catalysts.

Acknowledgements

We thank the support from Wenzhou Medical College, Case Western Reserve University, NSF (CMMI-1000768), AFOSR (FA9550-10-1-0546, FA9550-12-1-0069), AFOSR MURI (FA9550-12-1-0037), AFRL (FA8650-07-D-5800) through UTC (11-S587-100-01-C1), AFOSR-NBIT (FA2386-10-1-4071), the Zhejiang Innovation Team from Department of Education (T200917), the Ministry of Science and Technology of China (2009DFB30380), the Ministry of Education of China (IRT1077 and 211069), and the National "Thousand Talents Program" of China.

Notes and references

1 M. J. Allen, V. C. Tung and R. B. Kaner, *Chem. Rev.*, 2010, **110**, 132–145.
2 J. S. Bunch, A. M. van der Zande, S. S. Verbridge, I. W. Frank, D. M. Tanenbaum, J. M. Parpia, H. G. Craighead and P. L. McEuen, *Science*, 2007, **315**, 490–493.
3 K. S. Novoselov, A. K. Geim, S. V. Morozov, D. Jiang, Y. Zhang, S. V. Dubonos, I. V. Grigorieva and A. A. Firsov, *Science*, 2004, **306**, 666–669.
4 Y. B. Zhang, Y. W. Tan, H. L. Stormer and P. Kim, *Nature*, 2005, **438**, 201–204.
5 A. A. Balandin, S. Ghosh, W. Z. Bao, I. Calizo, D. Teweldebrhan, F. Miao and C. N. Lau, *Nano Lett.*, 2008, **8**, 902–907.
6 Y. W. Zhu, S. Murali, M. D. Stoller, K. J. Ganesh, W. W. Cai, P. J. Ferreira, A. Pirkle, R. M. Wallace, K. A. Cychosz, M. Thommes, D. Su, E. A. Stach and R. S. Ruoff, *Science*, 2011, **332**, 1537–1541.
7 F. Du, D. S. Yu, L. M. Dai, S. Ganguli, V. Varshney and A. K. Roy, *Chem. Mater.*, 2011, **23**, 4810–4816.
8 Z. Chen, W. Ren, L. Gao, B. Liu, S. Pei and H. M. Cheng, *Nat. Mater.*, 2011, **10**, 424–428.
9 K. P. Gong, F. Du, Z. H. Xia, M. Durstock and L. M. Dai, *Science*, 2009, **323**, 760–764.
10 S. Y. Wang, E. Iyyamperumal, A. Roy, Y. H. Xue, D. S. Yu and L. M. Dai, *Angew. Chem., Int. Ed.*, 2011, **50**, 11756–11760.
11 L. T. Qu, Y. Liu, J. B. Baek and L. M. Dai, *ACS Nano*, 2010, **4**, 1321–1326.
12 Z. S. Wu, A. Winter, L. Chen, Y. Sun, A. Turchanin, X. L. Feng and K. Müllen, *Adv. Mater.*, 2012, **24**, 5130–5135.
13 L. S. Panchakarla, K. S. Subrahmanyam, S. K. Saha, A. Govindaraj, H. R. Krishnamurthy, U. V. Waghmare and C. N. R. Rao, *Adv. Mater.*, 2009, **21**, 4726–4730.
14 S. Reich, A. C. Ferrari, R. Arenal, A. Loiseau, I. Bello and J. Robertson, *Phys. Rev. B: Condens. Matter Mater. Phys.*, 2005, **71**, 205201.
15 S. Suzuki and H. Hibino, *Mater. Sci. Eng., B*, 2011, **177**, 233–238.
16 L. Y. Zhao, R. He, K. T. Rim, T. Schiros, K. S. Kim, H. Zhou, C. Gutiérrez, S. P. Chockalingam, C. J. Arguello, L. Pálová, D. Nordlund, M. S. Hybertsen, D. R. Reichman, T. F. Heinz, P. Kim, A. Pinczuk, G. W. Flynn and A. N. Pasupathy, *Science*, 2011, **333**, 999–1003.
17 L. J. Ci, L. Song, C. H. Jin, D. Jariwala, D. X. Wu, Y. J. Li, A. Srivastava, Z. F. Wang, K. Storr, L. Balicas, F. Liu and P. M. Ajayan, *Nat. Mater.*, 2010, **9**, 430–435.
18 Z. Q. Li, C. J. Lu, Z. P. Xia, Y. Zhou and Z. Luo, *Carbon*, 2007, **45**, 1686–1695.
19 B. M. Concha, M. Chatenet, C. Coutanceau and F. Hahn, *Electrochem. Commun.*, 2009, **11**, 223–226.
20 P. G. Collins, K. Bradley, M. Ishigami and A. Zettl, *Science*, 2000, **287**, 1801–1804.
21 S. Y. Kim, J. Park, H. C. Choi, J. P. Ahn, J. Q. Hou and H. S. Kang, *J. Am. Chem. Soc.*, 2007, **129**, 1705–1716.
22 Y. Hernandez, V. Nicolosi, M. Lotya, F. M. Blighe, Z. Sun, S. De, I. T. McGovern, B. Holland, M. Byrne, Y. K. Gun'Ko, J. J. Boland, P. Niraj, G. Duesberg, S. Krishnamurthy, R. Goodhue, J. Hutchison, V. Scardaci, A. C. Ferrari and J. N. Coleman, *Nat. Nanotechnol.*, 2008, **3**, 563–568.
23 L. Yang, S. Jiang, Y. Zhao, L. Zhu, S. Chen, X. Wang, Q. Wu, J. Ma, Y. Ma and Z. Hu, *Angew. Chem., Int. Ed.*, 2011, **50**, 7132–7135.
24 S. B. Yang, X. L. Feng, X. C. Wang and K. Mullen, *Angew. Chem., Int. Ed.*, 2011, **50**, 5339–5343.
25 R. L. Liu, D. Q. Wu, X. L. Feng and K. Mullen, *Angew. Chem., Int. Ed.*, 2010, **49**, 2565–2569.

